frontiers | Frontiers in Earth Science

TYPE Original Research
PUBLISHED 10 March 2023
DOI 10.3389/feart.2023.1104631

OPEN ACCESS

EDITED BY
Antonio Simonetti,
University of Notre Dame, United States

REVIEWED BY
Sean McClenaghan,
Trinity College Dublin, Ireland
Wei Chen,
China University of Geosciences Wuhan, China

*CORRESPONDENCE
Bo Li,
libo1964@sina.com

SPECIALTY SECTION
This article was submitted to Geochemistry, a section of the journal Frontiers in Earth Science

RECEIVED 21 November 2022
ACCEPTED 28 February 2023
PUBLISHED 10 March 2023

CITATION
Liang X, Li B, Zhang X, Qin H, Li G and Zhang C (2023), Trace element composition and genesis mechanism of the Fuli Pb-Zn deposit in Yunnan: LA-ICP-MS and *in situ* S-Pb isotopic constraints.
Front. Earth Sci. 11:1104631.
doi: 10.3389/feart.2023.1104631

Trace element composition and genesis mechanism of the Fuli Pb-Zn deposit in Yunnan: LA-ICP-MS and *in situ* S-Pb isotopic constraints

Xingyu Liang[1], Bo Li[1]*, Xinyue Zhang[2], Huaikun Qin[3], Gao Li[3] and Chengnan Zhang[4]

[1]Faculty of Land Resource Engineering, Kunming University of Science and Technology, Kunming, China, [2]Kunming Geological Prospecting Institute, China Metallurgical Geological Bureau, Kunming, China, [3]Fuli Lead-Zinc Mine Co., Ltd., Fuyuan, China, [4]Yunnan Tin Industry Group (Holding) Company Limted R&D Center, Kunming, China

The Fuli Pb-Zn deposit in Yunnan is located in the southeast of the Sichuan-Yunnan-Guizhou (SYG) Pb-Zn metallogenic province in South China. Lead and zinc reserves total approximately 0.3 million tons with an average grade of 18.68% Pb+Zn. The stratiform ore occurs in the interlayer fracture zone of the middle Permian Yangxin formation dolomite. The main sulfides of the Fuli Pb-Zn deposit consist of sphalerite, galena, and pyrite, while dolomite and calcite are the main gangue minerals. Mineralization exhibits massive, disseminated, vein and breccia textures. Sphalerites of two colors (black and red) have been identified in the Fuli deposit. LA-ICP-MS analysis revealed that the black and red sphalerites were enriched in Cd, Cu, Ga, and Ge and depleted in Fe, Mn, and In to varying degrees. The aforementioned elements exhibit homogeneous patterns in the LA-ICPMS time resolution profiles, which is consistent with variations in the concentrations of major elements like Zn and S. This indicates that these elements may occur in sphalerite as a result of isomorphous substitution. However, elements such as As, Sb, Pb, and Ag fluctuate greatly in the LA-ICPMS time resolution profiles, suggesting that these elements may exist as fine inclusions. Thus, the different colors of the Fuli sphalerite may be attributed to various elements such as Ni, Cu, and Ga; Ni and Cu result in purple Sp, Cu renders sphalerite red, and Ga imparts a yellow color. The sulfur isotope compositions of the two sphalerites exhibit little variation, with $\delta^{34}S$ values ranging from 15.57‰ to 16.91‰, indicating the enrichment of ^{34}S. These results are consistent with the sulfur isotopic compositions of Permian marine sulfates, indicating that thermochemical sulfate reduction was the main source of the reduced sulfur in the hydrothermal fluids. *In situ* Pb isotopic composition analysis revealed $^{208}Pb/^{204}Pb$, $^{207}Pb/^{204}Pb$, and $^{206}Pb/^{204}Pb$ values for galena in the range of 38.5–38.651, 15.666–15.733, and 18.539–19.124, respectively. The *in situ* Pb isotopic ratios of most galenas plot on the field of the basement metamorphic rocks of the Kunyang Group. These *in situ* Pb isotopic signatures reveal that the metallogenic metals are mainly derived from crustal basement. The findings of this study suggest that the Fuli Pb-Zn deposit is a MVT Pb-Zn deposit controlled by the interlayer compressional structure with characteristics of carbonate-hosted, epigenetic, simple mineral symbiosis, high Pb-Zn grade, and abundant Cd, Ga, and Ge along with other dispersed elements.

KEYWORDS

LA-MC-ICPMS, *in situ* S-Pb isotopic, genesis mechanism, isotope geochemistry, sichuan-yunnan-guizhou Pb-Zn metallogenic province

1 Introduction

In the southwestern block of the Yangtze craton, South China, the Sichuan-Yunnan-Guizhou (SYG) metallogenic province hosts world-class carbonate-hosted Pb-Zn deposits, which are mostly associated with low-temperature fluids (<300°C) (Huang et al., 2011; Hu et al., 2017; Zhou et al., 2018b). The Pb-Zn deposits in this area mainly occur in a range of carbonate rocks from the Neoproterozoic Sinian Dengying Formation to the Late Paleozoic Permian Yangxin Formation. These deposits are characterized by high Pb and Zn grades along with enrichment in Cd, Ge, Ga, etc. Mineralization, which is generally structurally controlled by faults and folds, is interpreted as epigenetic and controlled by

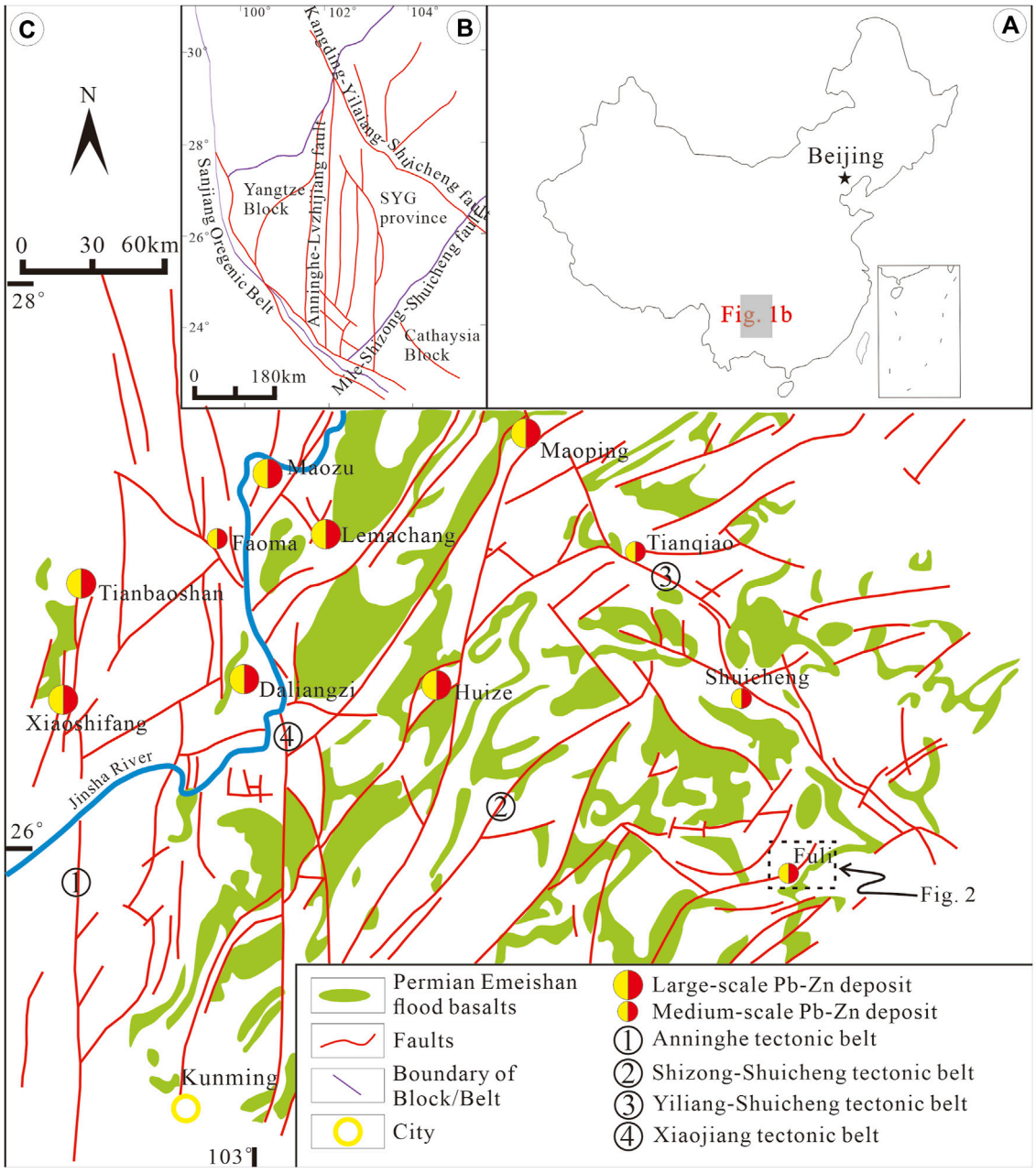

FIGURE 1
(A) A map showing the location of the SYG metallogenic province. **(B)** Geological framework of Southwestern China. **(C)** Geological map showing the distribution of the Pb-Zn deposits and Emeishan Flood basalt of the SYG metallogenic province, and the location of the Fuli deposit in the region.

the fault–fold structural system (Zhou et al., 2015; 2018a; Jin et al., 2016; Li, 2016; Cui et al., 2018).

The Fuli Pb-Zn deposit is located in the southeast of the SYG Pb-Zn metallogenic province (Figure 1). The orebody is stratiform and occurs in the Interlayered Fracture zone of Middle Permian Yangxin Formation Dolomite. There are few studies and reports available on this deposit. Sphalerite is the primary mineral of the Pb-Zn deposit, and it contains numerous trace elements, including Au, Ag, Cu, As, and Sb, as well as scattered elements such as Ge, Cd, Se, Te, and Tl, providing rich geochemical information (Fleet et al., 1993; Tu et al., 2003; Xu et al., 2014; Wei et al., 2019; 2021, 221). Isotope analyses are an effective way to trace the sources of ore-forming materials and is widely used to study the genesis of ore deposits; however, the origins revealed by single isotopes are often contradictory, and the mutual restriction of multi-isotope systems has become a development trend (Huang et al., 2004; Zhou et al., 2013d). Studying the trace elements and S and Pb isotopic compositions of sphalerite can not only reveal the sources of ore-forming materials, but also indicate the compositions of fluids and the geneses of ore deposits (Barker et al., 2009; Ye et al., 2011; Jin et al., 2016; Deng et al., 2017). LA-ICP-MS *in situ* analysis has advantages over traditional trace element analysis because it overcomes the problem of sample bias and dilution caused by sample selection. Moreover, LA-ICP-MS can efficiently determine the spatial distributions of trace elements in samples.

In this paper, LA-MC-ICP MS is used to determine the compositions of trace elements *in situ* along with the enrichment regularity of scattered elements and the S and Pb isotopes in the Fuli Pb-Zn deposit. The compositions and distributions of trace elements and scattered elements in sphalerite and the source of the ore-forming materials are discussed. The findings improve our understanding of the mineralization of ore deposits in the study region and provide a new theoretical basis for determining the genesis of Pb-Zn deposits.

2 Geological setting

2.1 Tectonic features of the fuli district

The Fuli Pb-Zn deposit is located 32 km southeast of Fuyuan County, Yunnan Province. It is controlled by the Qujing fault and a secondary splay of the Mile-Shizong fault (Figure 1). In the study region, the Kunyang Group is exposed as the basement; however, sediments from the Sinian to Silurian are missing above the Kunyang Group. This area exhibits three distinct types of structural belts: NS trending, NE trending, and NW trendingFollowing the Jinning, Caledonian, and Hercynian movements, the structures in this region are primarily north-south in orientation, followed by structures of a northeastern orientation. The NW-trending structures developed rapidly during the Yanshan-Himalayan tectonic movement and gradually formed the present-day north-south oriented structures, follow by the NE-trending structure and NW-trending structure. The structures that are oriented north-south and north-east play an essential role in determining the formation of Pb-Zn deposits, as well as their distribution and enrichment, in this region.

This region's geology is primarily determined by the Maitreya-Shizong fault. Several gentle anticlines, synclines, and reverse fault structures with a severe dip are dispersed across the mining area. Together, the Erle and Xinjuntai anticlines make up the principal fold structure in this region. The distribution of regional strata, secondary structures, and mineralization is governed by both faults and anticlines.

Among the approximate NS trending, NE trending and approximate EW trending structures developed in the mining area, the near NS trending faults have a large scale, which is a multi-stage active regional fault and an important ore fluid transporting structure, while the EW trending faults are small in scale and mostly secondary structures, mainly post-metallogenic structures. The NE trending faults are mainly ore-controlling structures, and a series of extensional fissures and interlayer fracture zones are produced in the strata of the middle Yangxin formation (P_2y^2), which provides a favorable structural trap for the emplacement of the Fuli Pb-Zn orebody. The orebodies mainly occur in these fissures and interlayer fracture zones (Ren et al., 2019).

2.2 Deposit geology

The study area suffered transgression cycles in the early and middle Permian, forming extremely thick carbonate strata. The exposed strata in the mining area are distributed along a N-S trend direction (Figure 2A). From oldest to youngest, the host strata are as follows: interbeds of limestone and dolomite of the Middle Permian Yangxin Formation (P_2y), Upper Permian Emeishan basalt ($P_2\beta$), Upper Permian calcareous and argillaceous shale of the Xuanwei Formation (P_3x), yellow brown mudstone and Lower Triassic shale of the Feixianguan Formation (T_1f), and argillaceous dolomite and limestone of the Yongningzhen Formation (T_1y). Mudstone and dolomite of Middle Triassic Guanling Formation (T_2g^1). The Yangxin Formation of the Middle Permian is the main deposit-bearing stratum. At present, two orebodies have been found in the Fuli Pb-Zn deposit: they mainly occur in dolomitic limestone, the orebodies are controlled by strata, and the metal content of zinc is the highest, with lead contents subordinate to zinc. It is approximately 320 m long, 210 m wide, and 1.2 m thick, with a SE dip of 15°. The orebody has the characteristics of being of greater thickness in the middle and thin at both ends. Shallow parts of the orebody are thin and the metal content are low, becoming thicker with higher Zn-Pb grades at depth (Figure 2B).

Through examination of geological characteristics and the microscopic observation of mineral associations, the genesis of the Fuli lead-zinc deposit can be separated into three phases: the early-mineralization stage, the syn-mineralization stage, and the post-mineralization stage (Figures 3, 4):

1) Early-mineralization period: The main feature of the ore is characterized by two distinct types of hydrothermal dolomitization in the early-mineralization period: Dol-1 and Dol-2. The Dol-1 dolomite appears as grey-black, fine-grained xenomorphic granules and often cemented by ore-forming grey dolomite (Figure 3D). The Dol-2 dolomite has a euhedral white core and a dark grey-grey edge with coarse particles. Sphalerite

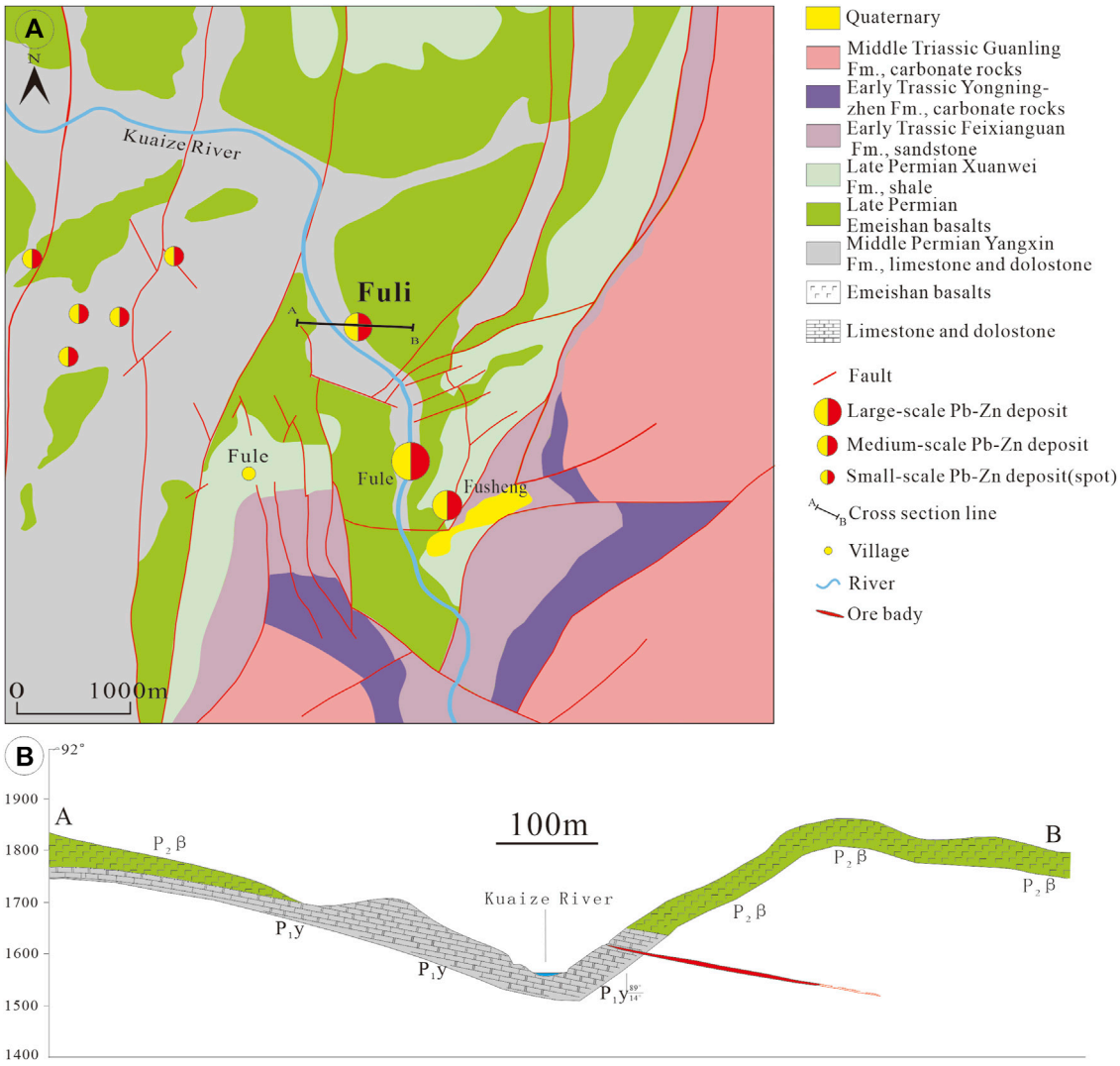

FIGURE 2
(A) Geological map of the Fuli Pb–Zn deposit showing the structure and the A-B cross-section. **(B)** A-B Cross-section of the Fuli deposit through the Fuli deposit showing the ore body, structure and strata.

and galena are found as bulk or disseminated replacements in the dolomite (Figures 3C, F).

2) Syn-mineralization period: The occurrence of minerals formed in the syn-mineralization period is consistent with that of the strata and developed in the interlayer fracture zone. The main minerals are sphalerite in massive, vein or disseminated forms, and galena as cubic crystal. In general, the sulfides have a granular texture (Figure 5A, B, E), metasomatic texture (Figures 5C, D, F), and some have formed massive structures, disseminated structures (Figure 3A), breccia structures (Figure 3B), and vein structures (Figure 3E). At this stage, the sphalerite is predominantly reddish-brown to brown-black, and its crystals are predominantly euhedral and anhedral.
3) Post-mineralization period: The euhedral calcite (Cal-5) is a gangue mineral generated in the post-mineralization stage. It is in the shape of a coarse vein and envelops sphalerite and galena in the syn-mineralization stage. (Figures 3B,E).

3 Methods

3.1 LA-ICP-MS elemental measurement

LA-ICP-MS was used to analyze the trace elements in minerals at Wuhan Sample Solution Analytical Technology Co., Ltd. (Wuhan, China). The operating conditions and data reduction for the laser system and the ICP-MS instrument were the same as described in (Zong et al., 2017). A GeolasPro laser ablation system was used to perform the sampling, which comprises a COMPexPro 102 ArF excimer laser (wavelength of 193 nm, maximum energy of 200 mJ) and a MicroLas optical system. For the acquisition of ion signal intensities, an Agilent 7700e ICP-MS instrument was utilized. In this experiment, helium was used as a carrier gas. The make-up gas was argon, which was mixed with the carrier gas *via* a T-connector prior to entering the ICP system. A "wire" signal-smoothing device was included in the laser ablation system (Hu

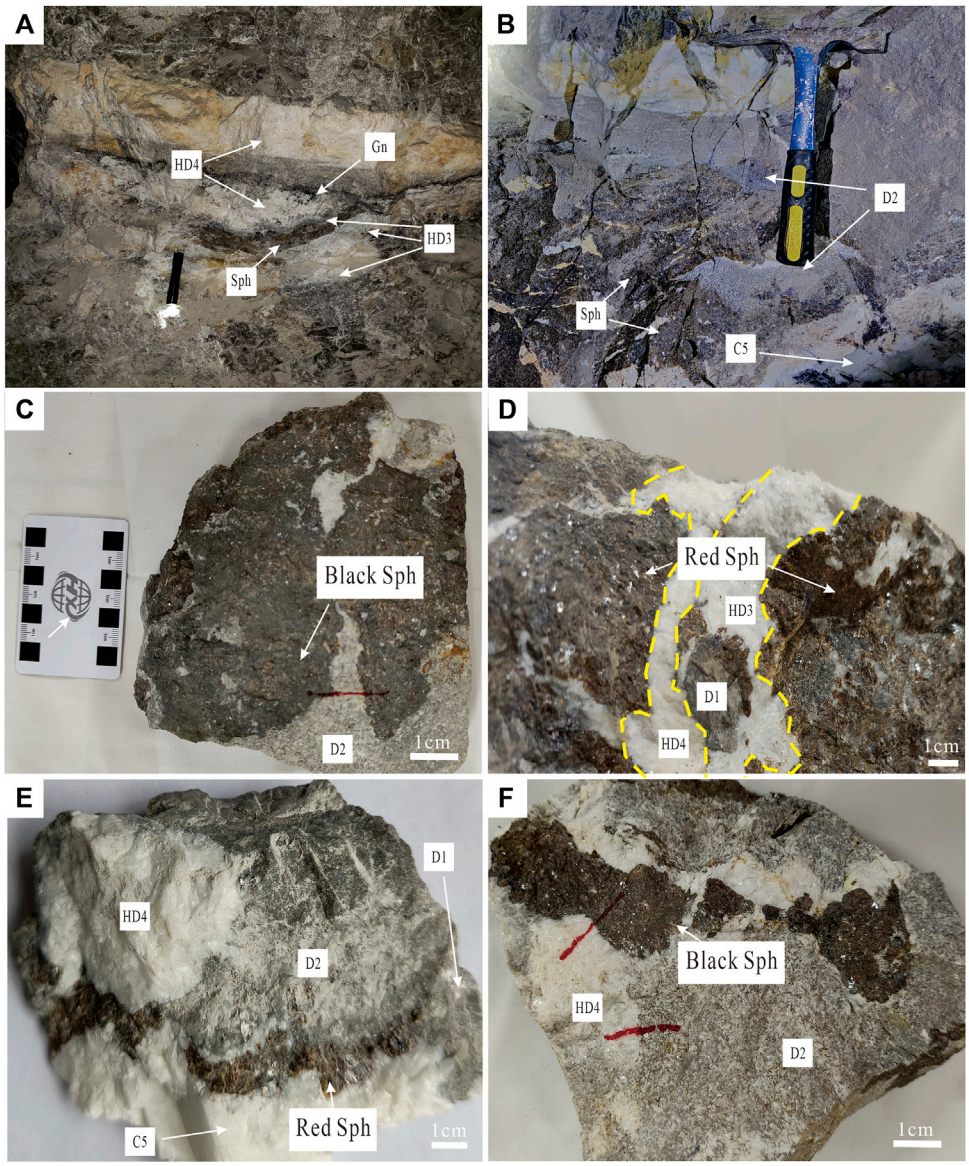

FIGURE 3
Photographs of field and specimens from the Fuli Pb-Zn deposit. **(A, B)** Bulk Sp and/or Gn are cemented by Dol/Cal veins. **(C)** Massive black sphalerite. **(D)** Massive red sphalerite. **(E)** Black sphalerite veins filled in dolomite fissures. **(F)** Black sphalerite breccia in hydrothermal dolomite vein.

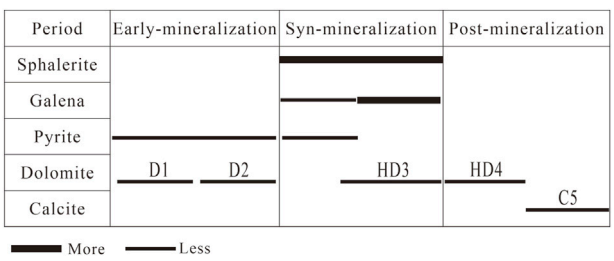

FIGURE 4
Paragenesis sequence of minerals in the Fuli Pb-Zn deposit.

et al., 2015). A spot size of 44 microns, a fluence of 5 J/cm^2 and a frequency of 5 Hz were used for experimental conditons. The trace element compositions of sulfides were calibrated against various reference materials (NIST 610 and NIST 612) without using an internal standard (Liu et al., 2008). To verify the accuracy of the calibration method, a sulfide reference material (MASS-1, USGS) was used as the unknown sample. The background acquisition for each analysis was approximately 20–30 s, followed by the acquisition of data from the sample for 50 s. A software program ICP-MS-DataCal v12.2 based on Excel was used to perform off-line selection and integration of the background and analyzed signals, as well as time-drift correction and quantitative calibration for the analysis of trace elements (Liu et al., 2008).

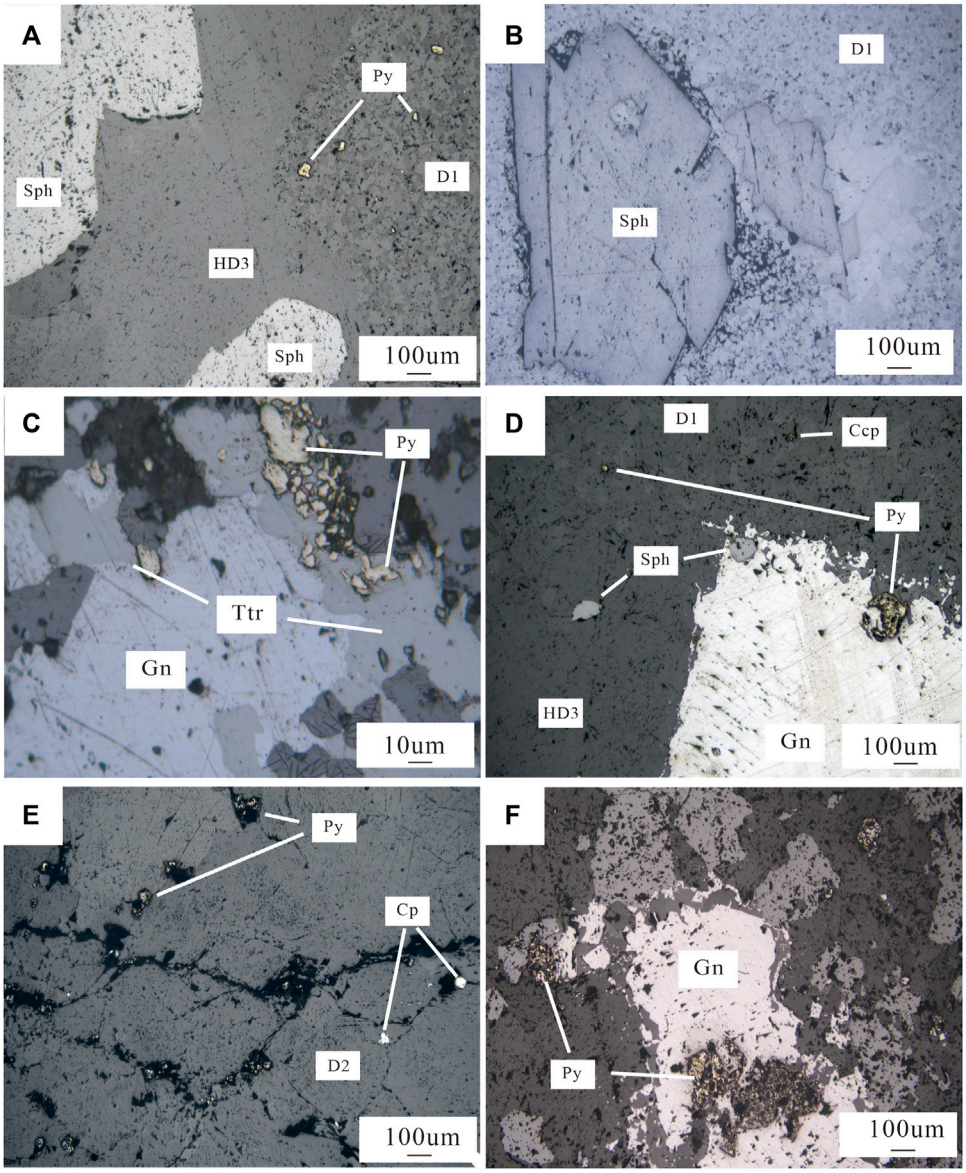

FIGURE 5
Sulfide mineral textures and structures from the Fuli Pb-Zn deposit. **(A)** Dolomite coexists with sphalerite. **(B)** Sphalerite with a granular structure. **(C, D)** Galena metasomatic pyrite and/or tetrahedrite. **(E)** Pyrite and chalcopyrite observed as bulk or disseminated in the dolomite **(F)** Metasomatic relict pyrite and xeno-morphic sphalerite in anhedral sphalerite fracture.

3.2 *In situ* sulfur isotope analysis

In situ sulfur isotope analyses of sphalerite were conducted using a Neptune Plus MC-ICP-MS instrument (Thermo Fisher Scientific, Bremen, Germany) and a Geolas HD excimer ArF laser ablation system (Coherent, Göttingen, Germany) at Wuhan Sample Solution Analytical Technology Co., Ltd. (Hubei, China). The laser ablation system utilized helium as the carrier gas for the ablation cell, which was then mixed with argon (the makeup gas) once it had left the ablation cell. During the ablation process, the single-spot mode was employed. To counteract the downhole fractionation effect, a large spot size of 44 μm and a slow pulse frequency of 2 Hz were used, as reported by (Fu et al., 2016).100 laser pulses were utilized in one analysis. Signal-smoothing devices were used downstream from the sample cell to effectively eliminate short-term variations in the signal, particularly for slow pulse frequencies (Hu et al., 2015). The laser fluence was maintained at a constant level of 5 J/cm^2. Nine Faraday cups with $10^{11}\Omega$ resistors were mounted on the Neptune Plus instrument. The ^{32}S, ^{33}S, and ^{34}S isotopes were collected in Faraday cups in static mode. For improved signal intensity, the Neptune Plus instrument utilizes the newly developed X skimmer cone and Jet sample cone. To reduce polyatomic interference, nitrogen was added to the central gas flow at a rate of 4 mL/min. Measurements were conducted at medium resolution with a revolving power of greater than 5,000, as defined by peak edge widths between 5% and 95% of peak height.

An instrument mass fractionation correction was conducted using standard sample bracketing (SSB). To eliminate the matrix effect, the natural pyrite, pyrrhotite, pentlandite samples, the natural chalcopyrite samples, and the natural Ag_2S samples, were corrected using a pyrite standard (PPP-1), a pressed pellet chalcopyrite standard (GBW07268), and a synthetic Ag_2S pressed pellet standard (IAEA-S-1), respectively. The reference values of δ^{34}Sv-CDT in these standards were reported by Fu et al. (2016). In addition, the in-house references of a pyrrhotite (SP-Po-01, δ^{34}Sv-CDT = 1.4 ± 0.4), chalcopyrite (SP-CP-01, δ^{34}Sv-CDT = 5.45 ± 0.3), and two synthetic Ag2S standards (IAEA-S-2, δ^{34}Sv-CDT = 22.58 ± 0.39 and IAEA-S-3, δ^{34}Sv-CDT = −32.18 ± 0.45) were analyzing repeatedly as unknown samples to verify the accuracy of the calibration method. A detailed description of the *in situ* analysis of the S isotopic ratios can be found in Fu et al. (2016). All data reduction for the MC-ICP-MS analysis of S isotopic ratios was conducted using Iso-Compass software (Zhang et al., 2020).

3.3 *In situ* lead isotope analysis

In situ lead isotope analyses of galena were conducted using a Neptune Plus MC-ICP-MS instrument (Thermo Fisher Scientific, Bremen, Germany) and a Geolas HD excimer ArF laser ablation system (Coherent, Göttingen, Germany) at Wuhan Sample Solution Analytical Technology Co., Ltd. (Hubei, China). The laser ablation system utilized helium as the carrier gas for the ablation cell, which was then mixed with argon (the makeup gas) once it had left the ablation cell. Depending on the intensity of the Pb signal, the spot diameter ranged from 44 μm to 90 μm. Pulses were delivered at a frequency of 8 Hz, while laser fluence was maintained at 10 J/cm^2. To eliminate short-term variations in the signal and to remove mercury from the background aerosol particles and sample aerosol particles, a new signal-smoothing and mercury-removing device was applied downstream from the sample cell (Hu et al., 2015). Nine Faraday cups with $10^{11}\Omega$ resistors were mounted on the Neptune Plus instrument. The ^{208}Pb, ^{207}Pb, ^{206}Pb, ^{204}Pb, ^{205}TL, ^{203}TL, and ^{202}Hg isotopes were collected in the Faraday cups in static mode. Using a Tl solution that was nebulized simultaneously with the sample using an Aridus II desolving nebulizer, the mass discrimination actor for Pb was calculated. The mass fractionation of Pb isotopes was adjusted based on the exponential rule and the ratio of ^{205}TL/^{203}TL. The optimized ^{205}TL/^{203}TL values obtained from the calibration of 2 Pb isotope standards MASS-1 (USGS) and Sph-HYLM (an in-house sphalerite standard), were substituted for the natural Tl isotopic composition when correcting for mass fractionation. The ^{202}Hg signal was used to correct the remaining ^{204}Hg interference on ^{204}Pb using the natural ^{202}Hg/^{204}Hg ratio (0.2301). A normalization of ^{205}TL/^{203}TL was performed to correct the mass fractionation of ^{204}Hg/^{202}Hg. ^{204}Hg/^{202}Hg and ^{205}TL/^{203}TL are assumed to have the same mass fractionation factors in this case. The precision and accuracy of the measurements were monitored using Sph-HYLM over the course of the analysis after 10 samples had been analyzed. For ^{208}Pb/^{204}Pb, ^{207}Pb/^{204}Pb, and ^{206}Pb/^{204}Pb, the achieved accuracy was judged to be equivalent to or more than 0.2‰ compared to the solution value measured by MC-ICP-MS. The typical precision was 0.4‰ (2σ). *In situ* analysis of Pb isotopic ratios is described in more detail in (Zhang et al., 2016). All data reduction for the MC-ICP-MS analysis of Pb isotope ratios was conducted using Iso-Compass software (Zhang et al., 2020).

4 Results

4.1 Trace elements of sphalerite

Table 1 summarizes the LA-ICP-MS trace element concentrations in sphalerites from the Fuli Pb-Zn deposit. Figure 6 shows a box-and-whisker graphic depicting the absolute concentration ranges for chosen elements.

4.2 Enrichment of Cu, Cd, Ge, and Ga

The contents of Cu, Cd, Ge, and Ga in sphalerite in the Fuli deposit are relatively high (Figure 6). The Cu content in the sphalerite samples ranges from 2.1 ppm to 3,390 ppm. The black sphalerite displays a higher Cu content (146 ppm–3390 ppm, with a mean value of 1,038 ppm) in comparison to the red sphalerite (2.1 ppm–2176 ppm, with a mean value of 499 ppm). The Cd content ranges greatly from 3,742 ppm to 25,238 ppm. The Cd content of black sphalerite (3,742 ppm–17475 ppm, mean value: 8,681 ppm) is lower than that of red sphalerite (5,532 ppm–25238 ppm, mean value: 12,443 ppm). The Ge content ranges from 0.22 ppm to 563 ppm. The black sphalerite exhibits a Ge content range of 20.6 ppm–563 ppm (with a mean value of 210 ppm), while the Ge content of red sphalerite ranges from 0.21 ppm to 230 ppm (mean value: 41 ppm). The Ga content ranges from 0.05 ppm to 674 ppm. The Ga contents of black sphalerite (2.2 ppm–674 ppm) and red sphalerite (0.05 ppm–582 ppm) are not significantly different.

4.3 Depletion of Fe, Ag, Sb, and Mn

The contents of Fe, Ag, Sb, and Mn in the sphalerite of the Fuli deposit are relatively low (Figure 6). The Fe content ranges from 1,166 ppm to 2,896 ppm. The Fe contents of black sphalerite (1,194 ppm–2,540 ppm, mean value: 1796 ppm) and red sphalerite (1,166 ppm–2,896 ppm, mean value: 1884 ppm) are not significantly different. The Ag content ranges from 0.12 ppm to 70 ppm. The Ag content of black sphalerite (0.39 ppm–70 ppm, mean value: 13.6 ppm) is higher than that

10.3389/feart.2023.1104631

TABLE 1 Summary of LA-ICP-MS sphalerites trace element concentration (ppm) in the Fuli Pb-Zn deposit.

Color	Sample no.	Cr	Mn	Fe	Co	Ni	Cu	Ga	Ge	As	Se	Ag	Cd	In	Sb	Tl	Pb
Black	FL1-1-1	0.89	0.71	1,224	12.9	2.3	939	5.1	130.5	14.5	7.7	13.1	10,001	0.26	471	0.22	873
	FL1-1-2	67.20	0.64	1,473	13.6	8.2	1,238	8.6	563.5	58.2	6.9	7.5	7,250	0.43	394	0.67	1,574
	FL1-1-3	0.27	1.49	1,360	13.2	6.6	1,377	6.8	277.2	117.0	11.0	3.0	8,628	0.41	347	0.32	243
	FL1-1-4	15.16	1.73	1,504	3.2	11.8	2,114	553.3	539.8	86.1	7.2	18.7	13,354	3.33	1,469	1.14	1,347
	FL1-1-5	1.09	0.53	1,455	9.8	0.6	814	2.2	351.0	25.6	1.1	1.9	4,614	0.05	93	0.03	41
	FL1-1-6	7.62	0.76	1708	9.2	0.3	146	2.5	20.6	20.0	0.0	1.2	7,786	1.02	55	0.11	2,911
	FL1-1-7	0.82	1.05	2,431	7.8	1.0	272	13.2	117.9	20.4	0.0	0.4	3,742	0.03	16	0.02	20
	FL2-1-1	3.34	0.83	1840	11.6	2.7	1,210	647.2	160.1	25.7	13.3	4.1	7,835	1.52	214	0.10	49
	FL2-1-2	1.63	0.80	1,363	9.2	0.7	1,396	36.9	463.4	96.9	0.0	6.2	5,247	0.39	400	0.05	135
	FL2-1-3	0.72	0.78	1781	9.0	0.8	309	10.9	76.8	32.6	11.8	3.8	6,791	0.10	125	0.01	51
	FL2-1-4	1.18	0.00	2082	10.4	0.7	3,391	673.9	262.1	254.8	0.0	69.8	9,386	0.32	2019	0.31	557
	FL2-1-5	1.24	0.46	1,194	10.0	0.6	292	69.1	60.1	14.4	0.0	2.4	5,783	0.21	99	0.05	27
	FL2-1-6	9.15	0.00	2,344	11.0	0.9	825	309.3	80.2	55.0	0.0	14.5	17,475	2.00	296	0.15	53
	FL2-1-7	2.04	0.85	2,279	11.3	0.8	614	73.7	50.3	66.1	2.9	34.0	8,384	0.07	389	0.12	131
	FL2-1-8	1.80	1.68	2,540	11.1	1.2	1,401	415.9	89.4	94.4	13.8	27.4	16,174	0.24	798	0.12	353
	FL2-1-9	1.85	0.77	1888	10.7	0.9	683	29.1	140.6	72.5	15.5	15.0	6,955	0.01	322	0.06	139
	FL2-1-10	1.38	0.00	2066	9.8	0.9	634	8.7	182.6	59.6	0.0	7.4	8,182	0.00	199	0.02	121
Red	FL1-3-1	1.67	0.98	2031	9.8	0.9	808	6.6	219.7	76.1	8.7	7.8	11,015	0.01	312	0.01	88
	FL1-3-2	0.91	0.74	1,675	9.7	0.6	946	84.9	230.1	72.0	0.0	7.0	8,004	0.33	379	0.03	167
	FL1-3-3	0.76	0.56	1,436	8.9	0.7	17	3.3	3.8	0.6	15.1	0.4	6,126	0.01	2	0.00	1
	FL1-3-4	0.00	0.00	1,693	9.9	0.6	103	4.1	18.5	9.4	0.0	2.3	5,532	0.00	51	0.02	12
	FL1-3-5	1.87	1.28	2,706	8.7	1.1	32	0.7	0.6	14.3	12.5	0.6	17,485	0.64	8	0.14	5
	FL1-3-6	3.99	0.96	2,896	8.9	1.3	79	0.0	0.2	0.0	0.0	1.9	19,370	0.02	3	0.00	13
	FL16-1-1	1.10	0.86	2,412	10.4	1.1	96	48.0	3.8	3.1	30.4	1.5	15,919	0.01	42	0.00	15
	FL16-1-2	1.50	1.39	2,117	10.5	1.0	141	92.5	9.1	4.1	10.1	1.3	25,238	0.01	49	0.00	26
	FL16-1-3	1.78	0.00	1,166	13.3	0.4	114	40.6	18.8	22.8	0.0	0.8	5,633	0.60	3	0.04	4
	FL16-1-4	1.15	1.08	1,662	11.9	0.8	2	0.1	0.4	0.5	0.0	0.1	16,152	0.00	1	0.00	1
	FL16-1-5	0.61	2.95	1984	12.6	2.4	975	8.2	3.4	3.9	10.5	0.7	10,701	0.13	179	0.13	44
	FL16-1-6	3.58	1.99	1767	13.3	2.7	647	2.6	4.3	13.6	10.6	1.3	7,617	0.15	79	0.12	28
	FL16-1-7	0.43	3.79	1,553	12.4	3.5	852	3.3	39.4	1.0	13.6	0.8	8,619	0.98	95	0.22	109
	FL16-1-8	1.34	2.36	1,278	0.8	1.8	2,176	582.3	24.1	6.2	20.8	1.7	16,796	0.85	173	0.40	180
Measured concentrations (ppm)																	

of red sphalerite (0.12 ppm–7.7 ppm, mean value: 2.02 ppm). The Sb content ranges from 1.21 ppm to 2019 ppm. The Sb content of black sphalerite ranges from 15.5 ppm to 2019 ppm (mean value: 453 ppm), while the Sb content of red sphalerite is relatively low (1.21 ppm–379 ppm, mean value: 98 ppm). The Mn content ranges from 0 to 3.79 ppm. The Mn contents of black sphalerite (0–1.73 ppm) and red sphalerite (0–3.79 ppm) are not significantly different. In summary, the contents of Cu, Ag, As, Ge, Pb, and Sb decreased from black sphalerite to red sphalerite.

4.4 $\delta^{34}S$ values

The in situ-measured $\delta^{34}S$ values of the black and red sphalerites are listed in Table 2. The $\delta^{34}S$ values of the sphalerites determined *in*

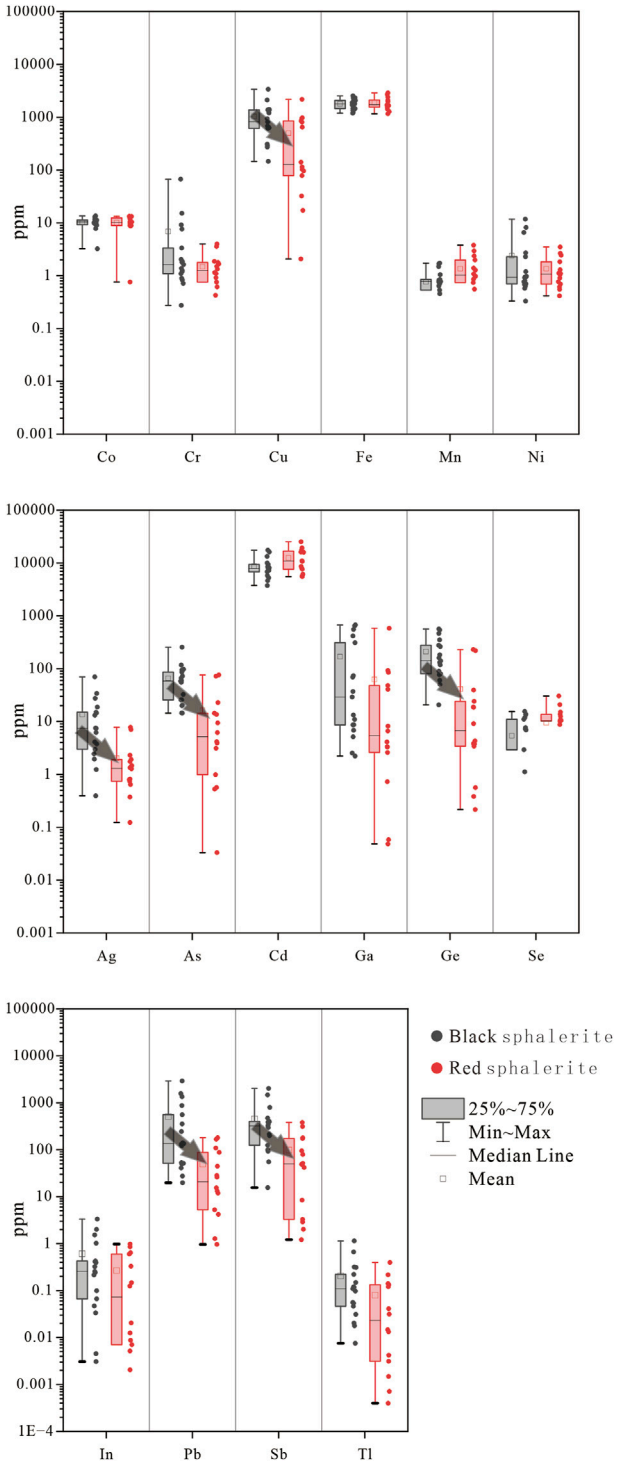

FIGURE 6
Box diagrams illustrating the concentration of trace elements in sphalerites from the Fuli Pb-Zn deposit.

situ by LA-ICP-MS range from +15.57‰ to +16.91‰. Significant differences are not observed in the $\delta^{34}S$ values of the black and red sphalerites (15.88‰–16.91‰ and 15.57‰–16.79‰, respectively), indicating similar sources.

TABLE 2 Summary of *in situ* S isotopic compositions in the Fuli Pb-Zn deposit.

Mineral	Color	Sample no.	$\delta^{34}S_V$-CDT (‰)
Sphalerite	Black	FL2-2	16.690
		FL6-1	16.500
		FL7-1	16.170
		FL9-1	16.910
		FL10-1	16.250
		FL11-1	16.580
		FL18-1	15.920
		FL18-2	15.880
	Red	FL1-3-01	16.790
		FL1-3-02	16.340
		FL16-1-01	16.200
		FL16-1-02	15.880
		FL16-2-01	16.280
		FL16-2-02	16.460
		FL16-2-03	15.760
		FL16-2-04	15.570

4.5 Pb isotopic compositions

The *in situ* measured Pb isotopic values of galena are listed in Table 3. The Pb isotopic composition of galena in the Fuli deposit varies little ($^{208}Pb/^{204}Pb$ = 38.5–38.651, $^{207}Pb/^{204}Pb$ = 15.666–15.733, and $^{206}Pb/^{204}Pb$ = 18.539–19.124). The narrow range of lead isotope values in galena and concentrated data imply similar source areas or high homogenization.

5 Discussion

5.1 Mechanisms of trace element incorporation in sphalerite

Among the trace elements found in the Fuli Pb-Zn deposit sphalerite, Cu, Fe, and Cd have the highest contents. The range of Fe and Cd contents is narrow, and these elements appear as homogeneous patterns in the LA-ICP-MS time resolution profiles; these are parallel to those of Zn and S (Figure 7), indicating that Fe and Cd occur in sphalerite *via* isomorphism. Since the ion radii of Fe^{2+}, Cd^{2+}, and Zn^{2+} are similar, these ions can replace each other in the sphalerite structure (Liu et al., 2015). In high-temperature environments, Fe has a strong ability to replace Zn *via* isomorphism. However, as the temperature decreases, Cd enters sphalerite and occupies the lattice position of the original Fe, resulting in a weak negative correlation between the contents of Cd and Fe in black sphalerite. However, red sphalerite is mostly formed in the middle and late stages of hydrothermal mineralization, when Cd and Fe mutually enter sphalerite; thus, a weak positive correlation is

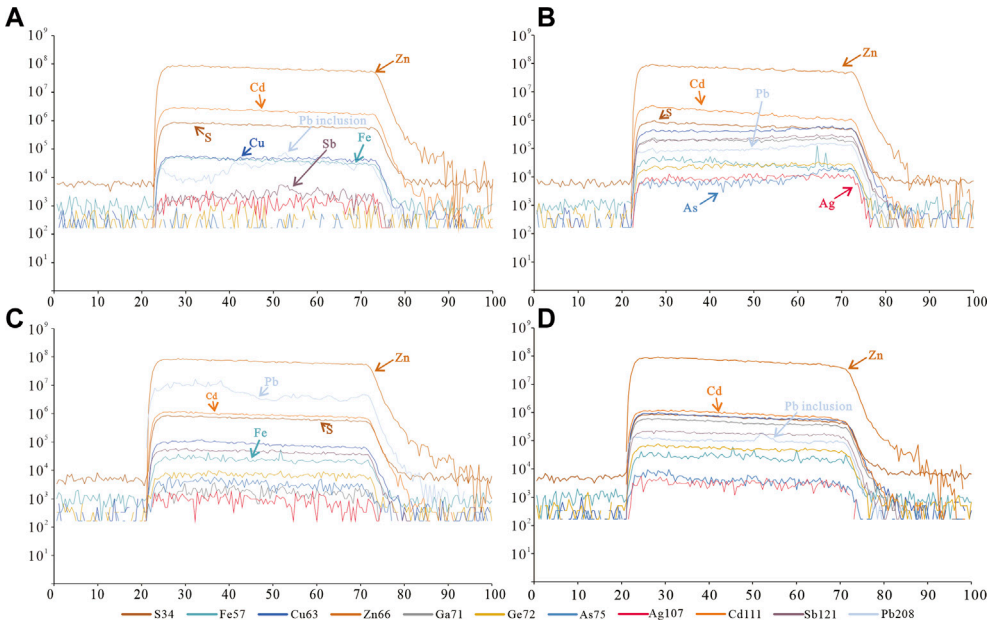

FIGURE 7
Representative time-resolved LA-ICP-MS depth profiles for sphalerite.

TABLE 3 Summary of *in situ* Pb isotopic compositions in the Fuli Pb-Zn deposit.

Mineral	Sample no.	$^{208}Pb/^{204}Pb$	$^{207}Pb/^{204}Pb$	$^{206}Pb/^{204}Pb$
Galena	FL2-1-01	38.563	15.700	18.563
	FL2-1-02	38.500	15.672	18.539
	FL2-1-03	38.542	15.684	18.634
	FL2-1-04	38.534	15.687	18.650
	FL2-1-05	38.534	15.687	18.623
	FL6-1-01	38.651	15.733	18.637
	FL7-1-01	38.552	15.695	18.563
	FL9-1-01	38.606	15.694	18.589
	FL10-1-01	38.543	15.690	18.558
	FL1-3-01	38.525	15.666	18.602
	FL1-3-02	38.576	15.680	18.544
	FL16-1-1	38.545	15.689	18.558
	FL16-1-2	38.568	15.676	18.555
	FL16-1-3	38.610	15.688	18.561
	FL16-1-4	38.606	15.692	18.565
	FL16-1-5	38.609	15.724	19.124
	FL16-1-6	38.601	15.705	18.759

observed between the contents of Cd and Fe in red sphalerite (Figure 8I).

Although the contents of Cu and Ge vary greatly in the red and black sphalerite, at most of the test points, the content of Cu exceeds 300ppm, and the content of Ge is more than 10 ppm. Meanwhile, Cu and Ge appear in a nearly homogeneous patternin the LA-ICPMS time resolution profile (Figure 7), and the range of Cu and Ge contents parallels that of Zn and S. This indicates that Cu and Ge may also exist as an isomorphic substitution in sphalerite. The tetrahedral covalent radii of Cu^{2+}, Zn^{2+}, and Ge^{2+} ions are 1.35, 1.31, and 1.22 respectively; thus, Cu^{2+} more easily enters the sphalerite lattice than Ge^{2+}. The average ion radius of the combination of the Cu^{2+} and Ge^{2+} is closer to the ion radius of Zn^{2+}, which is more conducive to the occurrence of isomorphic substitution and a possible mechanism is: $nCu^{2+}+Ge^{2+}\leftrightarrow(n+1)\ Zn^{2+}$ (Ye L et al., 2016). This possible mechanism has also been confirmed in this study: 1) identification of arsenic tetrahedrite and a small amount of chalcopyrite in the deposit (Figure 5C), indicating that the ore fluid was saturated in Cu at some stage; 2) a significant positive association exists between Cu and Ge in the Cu-Ge diagram (Figure 8), indicating that Cu and Ge entered sphalerite synchronously. This coupled substitution may be an important reason for the enrichment of Ge in sphalerite in this deposit. The contents of Ag and As in sphalerite are relatively low and vary greatly. In some LA-ICPMS time resolution profiles, Pb appears as an unsmooth curve, while the range of Ag, As, and Sb contents are parallel to Pb (Figure 7), indicating that Pb may exist in the form of fine-grained galena inclusions. However, Ag, As, and Sb may occur in galena micro-inclusions in the form of an isomorphic substitution.

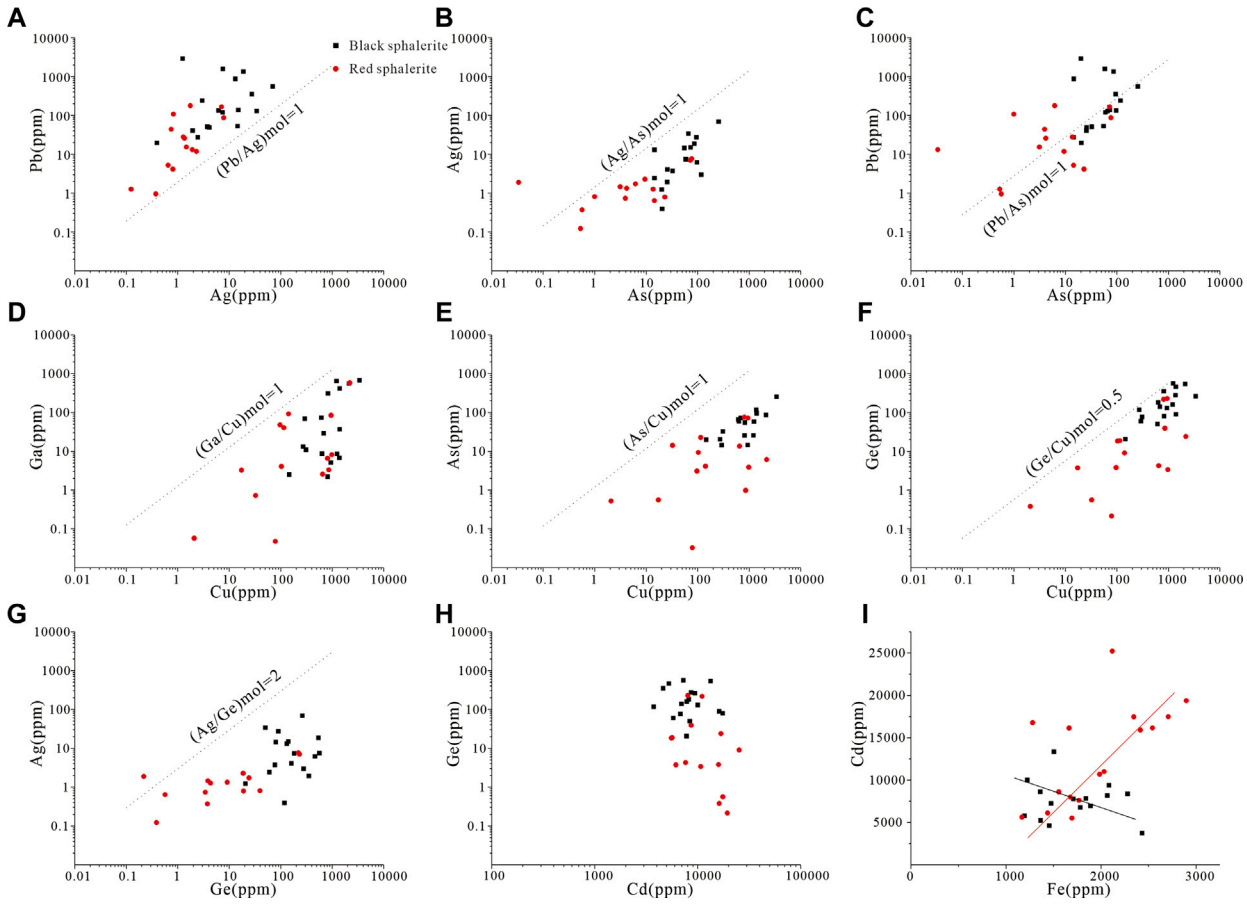

FIGURE 8
Binary plots illustrating the relationship of trace elements in sphalerite from the Fuli Pb-Zn deposit.

Previous work suggests that the varying sphalerite colors are related to the following factors. 1) With increases in the Fe content in sphalerite increases, its color changes from colorless to yellow, brown, or even black (Chen, 1979). 2) It can be caused by various impurity elements in natural sphalerite, including those related to the addition of Cu, Tl, and Cd (Toulmin et al., 1991). 3) Sphalerite may have other colors only when the Fe content is lower than 1%; whilst, yellow sphalerite may be related to the incorporation of Cu and Ga *via* isomorphism, and red sphalerite may be caused by the addition of elements such as Cu, Ga, and Hg (Li and Peng, 1990). In a systematic study of the nearby Fule deposit, the color of Fule sphalerite is related to various elements such as Ni, Cu, Tl, Ga, Hg, Fe, and Cr; Ni and Cu result in purple sphalerite, Cu results in red sphalerite, and Ga results in yellow sphalerite (Si, 2005). Our findings indicate that the contents of Fe in black and red sphalerite are similar (average Fe contents of 1795.993 ppm ppm and 1884.106ppm, respectively), implying that Fe may not affect the sphalerite color. Rather, the color may result from a combination of various factors. The variation in sulfur isotopes between the black and red sphalerites in this study is small, which does not affectthe sphalerite color. Generally, the microscopic color of sphalerite is uneven, and the overall color results from a combination of purple, red, yellow, and colorless varieties; thus, the change rule for trace elements in sphalerite of different colors is not significant (Si, 2005). The contents of Cu, Ag, As, Ge, Pb, and Sb decrease gradually from black sphalerite to red sphalerite, implying that these elements are more enriched in dark sphalerite.

5.2 Sources of reduced sulfur

There are three potential sources of sulfur sources in hydrothermal deposits. 1) Mantle-derived sulfur. Many materials are derived from the mantle, and it is not possible to directly determine the composition of mantle-derived S isotopes. The S isotope composition of chondrite is generally thought to be close to that of the mantle, and its $\delta^{34}S$ value is close to 0 (approximately 0‰ ± 3‰) (Chaussidon et al., 1989). 2) Seawater sulfur, which has a $\delta^{34}S$ value of approximately +20‰, although a significant amount of variation exists. It is widely recognized that the δ34S value of marine evaporites reflects the sulphur isotope composition of seawater sulphate. 3) Reduced (deposited) sulfur, characterized by its highly negative values of $\delta^{34}S$.

In the Fuli Pb-Zn deposit, the mineral assemblage is relatively simple; with the exception of sulfides such as sphalerite, galena, and

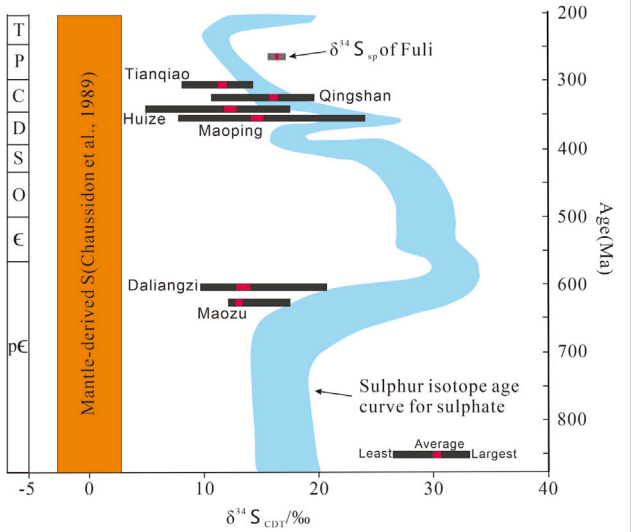

FIGURE 9
A comparison of sulfur isotopic compositions between the Pb-Zn deposits located in different strata ages of the SYG metallogenic province, seawater and mantle-derived sulfur (modified after Claypool et al., 1980). The data sourced from (Chaussidon et al., 1989; Huang et al., 2004; Zhou et al., 2010; 2013b; 2013c; 2013a; Yuan et al., 2014; Wei et al., 2021).

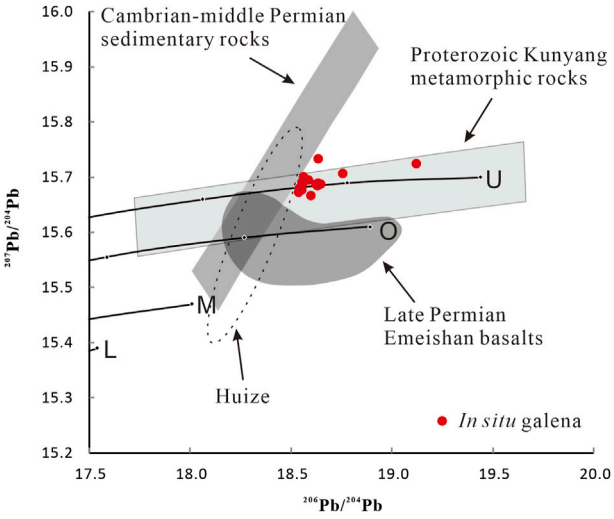

FIGURE 10
The comparison plot of $^{207}Pb/^{204}Pb$ vs. $^{206}Pb/^{204}Pb$ that display the field of late Permian Emeishan basalts, Cambrian-middle Permian sedimentary rocks and Proterozoic metamorphic rocks, and the Pb evolution curves of U, O, M and L (after Zartman and Doe, 1981); Upper Crust (U), Orogen Belt (O), Mantle (M) and Lower Crust (L). The data sourced from (Huang et al., 2004; Li et al., 2007; Yan et al., 2007; Zhou et al., 2013b; 2014; Bao et al., 2017).

a small amount of pyrite, no sulfate minerals are found. Therefore, the mean $\delta^{34}S$ value of sulfide approximately represents the $\delta^{34}S_{\sum S}$ value of the hydrothermal fluid (Ohmoto, 1972; Ohmoto and HGMB, 1997). The range of $\delta^{34}S$ values for the black and red sphalerite in the deposit is narrow (15.57‰–16.91‰, average = 16.261‰). These values are much higher than those of magmatic sulfates (Figure 9), ruling out the possibility that magmatism provided massive reduced sulfur. Evaporated gypsum strata are developed in many sedimentary strata where the deposit is located. These strata are rich in seawater sulfate minerals such as gypsum and barite, and their $\delta^{34}S$ values range from 22‰ to 28‰ (Huang et al., 2004; Zhou et al., 2013b; Jin et al., 2016), higher than those of Permian seawater sulfates (11‰–15‰) (Claypool et al., 1980), which are in good agreement with the $\delta^{34}S$ values observed in this study (Figure 9). The thermochemical reduction of sulfate minerals can lead to a Δsulfate-sulfide value (Seal, 2006; Zhou et al., 2013d) as high as 15‰. Thus, it can be concluded that the main sulfur source for Fuli Pb-Zn deposits is the seawater sulfate rock in sedimentary strata.

Sulfate reduction mainly occurs through two mechanisms: thermochemical sulfate reduction (TSR) and bacterial sulfate reduction (Ohmoto, 2018). Based on microthermometry, the homogenization temperatures of fluid inclusions in Fuli sphalerite is approximately 110°C–200°C (unpublished data) higher than that of bacterial reduction (Jørgensen et al., 1992). In addition, bacterial sulfate reduction will result in S isotope fractionation of 40% or more (relative to sulfate) (Ohmoto, 2018), which is inconsistent with the similar $\delta^{34}S$ values of

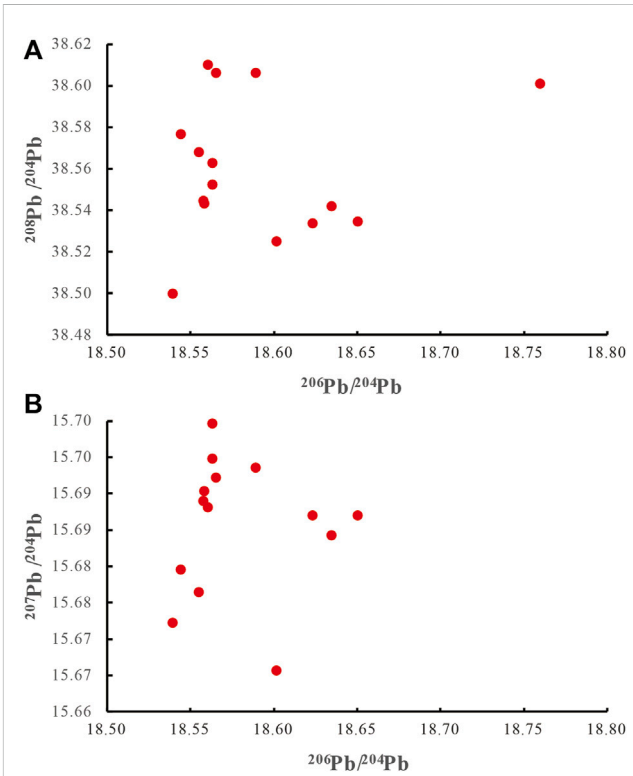

FIGURE 11
Plots of $^{208}Pb/^{204}Pb$ vs. $^{206}Pb/^{204}Pb$ **(A)** and $^{207}Pb/^{204}Pb$ vs. $^{206}Pb/^{204}Pb$ **(B)** of galena.

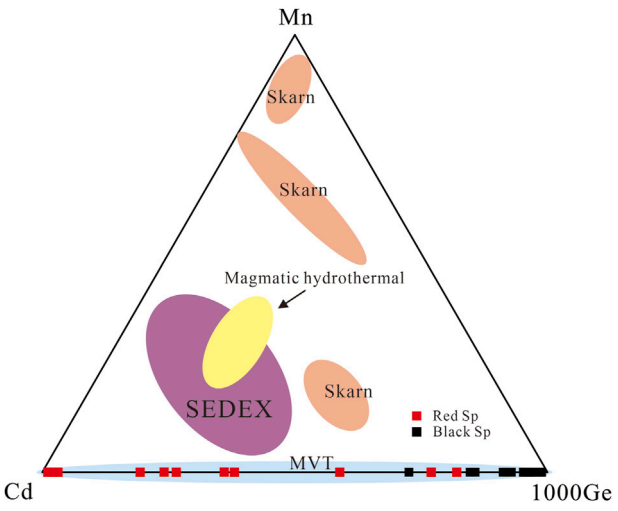

FIGURE 12
Ternary Cd–Mn–1000Ge plot of sphalerite from the Fuli deposit modified after (Zhou et al., 2022).

sulfates and sulfides in the deposit. At the same time, the sulfur isotopes in Fuli sphalerite range from 15.57‰ to 16.91‰, close to the $\delta^{34}S$ values of marine sulfate and regional underlying strata in the same period; thus, TSR may be the main mechanism of sulfur reduction in this deposit. A large amount of reducing sulfur can be produced through TSR within a short period of time (Ohmoto, 1972). There is no evident sulfur isotope fractionation (Ohmoto, 2018) between reduced sulfur and sulfate. The sulfur isotope fractionation coefficient between SO_4 and H_2S during TSR is considered to be 1.030 (Ottaway et al., 1994). The production efficiency of TSR is highest in the temperature range of 110°C–200°C (Ohmoto, 2018), commensurate with the temperature of fluid inclusion homogenization in Fuli sphalerite (Liang et al., 2022). Therefore, S^{2-} in the ore-forming fluid of the Fuli Pb-Zn deposit is most likely the product of marine sulfate mineral TSR.

5.3 Sources of metallic elements

The range of the *in situ* Pb isotopic compositions of galena in the Fuli Pb-Zn deposit is restricted (Table 3), implying a single source of ore-forming metals in the deposit or a mixed source with a high degree of homogenization (Huang et al., 2004; Zhou et al., 2018b). In the $^{207}Pb/^{204}Pb$-$^{206}Pb/^{204}Pb$ diagram (Figure 10), the galena in the Fuli Pb-Zn deposit has a uniform Pb isotope composition, and all the data plot near the Pb average evolution line of the upper crust. This further indicates a crustal source of the ore-forming materials. Plotting the lead isotopic composition of the regional crystalline basement (Kunyang Group), Emeishan basalt, Devonian-Permian carbonate sedimentary strata, and the Huize Pb-Zn deposit onto the $^{207}Pb/^{204}Pb$-$^{206}Pb/^{204}Pb$ diagram (Figure 10) indicates that the Pb isotopes of the deposit are mainly concentrated in the Pb isotopic range of the Kunyang Group; it's isotopic range is different from that of the Emeishan basalts. The Pb isotope data of sphalerite in the Fuli deposit displays a positive correlation tendency, implying that the sulfide Pb in the Fuli deposit may have a mixed source (Figure 11) (Canals and Cardellach, 1997). Si RJ (2005) and Zhou et al. (2018a)

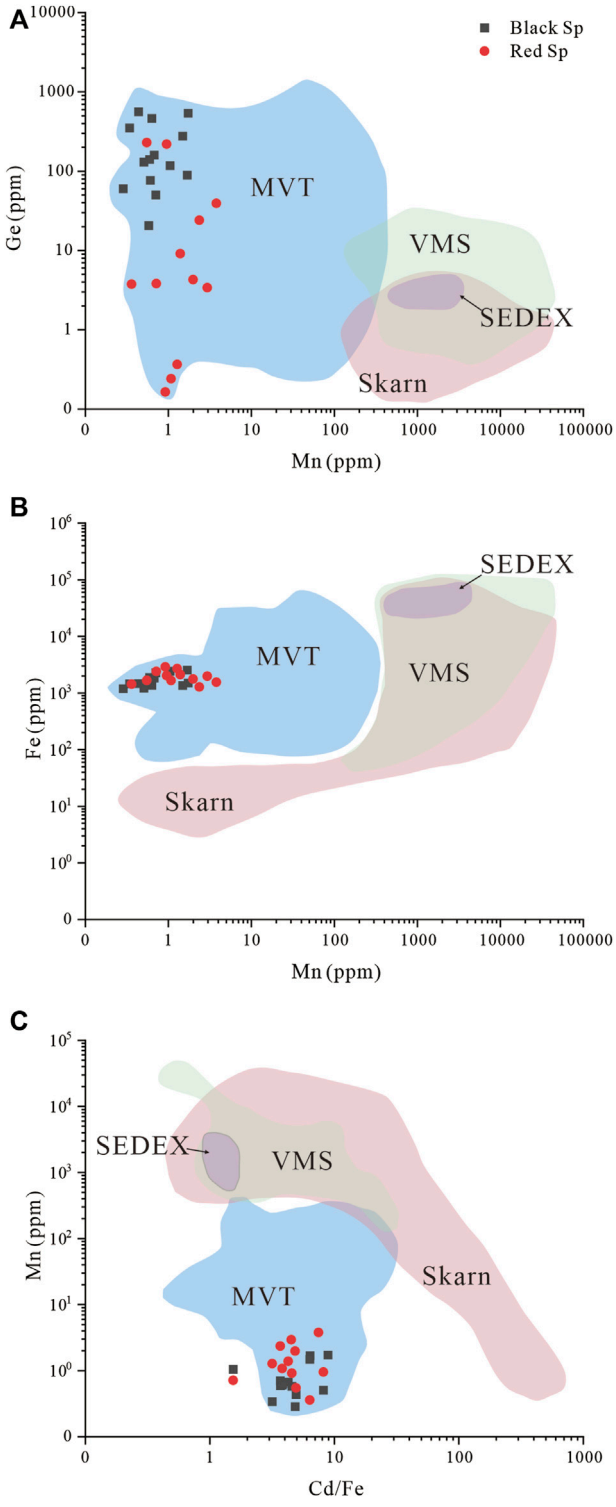

FIGURE 13
Binary plots of **(A)** Mn and Ge; **(B)** Mn and Fe; **(C)** Cd/Fe and Mn. These data are collected from (Cook et al., 2009; Ye L et al., 2016; Li et al., 2020; Wei et al., 2021; Yang et al., 2022).

also found that the Pb isotopes of adjacent deposits in this area have the characteristics of multiple sources. Combined with the regional geological and geochemical characteristics of the deposit, the metal elements of the Fuli Pb-Zn deposit may have multiple sources but originate principally from the Kunyang Group.

5.4 Ore genesis

The trace element composition of sphalerite can provide valuable information about the conditions under which they formed. For example, variations in the concentration of certain trace elements can be used to infer the temperature, pressure, fO2, and pH during mineral formation (Cook et al., 2009; Ye et al., 2011; Li et al., 2020). Additionally, the presence of certain trace elements in sphalerite can be used to track the source of the mineralizing fluids, and to determine whether they were derived from deep-seated magmatic sources or from shallower, sedimentary sources. Thus, the trace element composition of sphalerite can provide important clues about the origin and evolution of ore deposits.

The compositional characterization of trace elements in sphalerite has been widely applied as an effective tool for distinguishing various deposit types. Among the numerous trace elements present in sphalerite, Fe, Mn, Cd, Co, Ge, Ga have been particularly useful in identifying the origin and formation conditions of ore deposits. Specifically, sphalerite found in magmatic-related deposits is typically characterized by high concentrations of Fe, Mn, and Co, but lower levels of Ge and Cd. In contrast, sphalerite from Mississippi Valley Type (MVT) deposits typically displays low levels of Fe, Mn, and Co, but elevated concentrations of Ge, Cd, and Ga (Cook et al., 2009; Ye L et al., 2016; Wei et al., 2019; Hu et al., 2020; Li et al., 2020).

The Fuli Pb-Zn deposit has a simple mineral composition and a low degree of wall rock alteration. The mineralization is primarily Zn, and the ore-forming temperature is inferred to be low (110°C–200°C). The Pb-Zn orebody predominantly hosted in the dolomite of the Middle Permian Yangxin formation and is governed by fault structures. The Pb-Zn mineralization fills the fault fracture zone in a bedlike manner, and epigenetic mineralization is noticeable. These geological characteristics are similar to those of a classic MVT deposit (Leach et al., 2001; 2010), and the metallogenic characteristics are similar to those of other Pb-Zn deposits in the SYG area (Zhang, 2008). In the Cd–Mn–1000Ge (Figure 12), as well as in the Ge–Mn (Figure 13A), Fe–Mn (Figure 13B), and Mn–Cd/Fe (Figure 13C) discrimination plots, the Fuli sphalerite is located in the field that is indicative of MVT deposits. Compared with the typical MVT deposit, the content of Cu in this deposit is higher, and the chalcopyrite and tetrahedrite are distributed in a droplet-like manner within the sphalerite. Based on the field geologic characteristics, sphalerite trace elements, and S and Pb isotope geochemistry, the Fuli Pb-Zn deposit should belong a MVT type Pb-Zn deposit.

6 Conclusion

The main conclusions drawn from this study are summarized as follows:

1) Fe, Cd, Cu, and Ge in sphalerite may occur in the form of isomorphic substitutions, Pb may exist in the form of galena micro-inclusions, and Ag, As, and Sb may occur in galena micro-inclusions.
2) The contents of Cu, Ag, As, Ge, Pb, and Sb decrease gradually from black sphalerite to red sphalerite, and the color of sphalerite may change with the contents of Ni, Cu, Ga, and other elements.
3) Ore-forming fluids, sulfur was primarily derived from seawater sulfate rocks as a product of TSR, while ore-forming metals mainly come from basement rocks.
4) The Fuli Pb-Zn deposit occurs in the dolomite of the Middle Permian Yangxin formation and is controlled by the interlayer compressional structure. The characteristics of epigenetic ore are clear, the mineral composition is simple (mainly sphalerite, galena, and pyrite), and the Pb-Zn grade is high. The Fuli Pb-Zn deposit is enriched in Cd, Ga, Ge, and other dispersed elements. Based on the field geologic characteristics, sphalerite trace elements, and S and Pb isotope geochemistry, the Fuli Pb-Zn deposit should be classified as an MVT type Pb-Zn deposit.

Data availability statement

The original contributions presented in the study are included in the article/supplementary material, further inquiries can be directed to the corresponding author.

Author contributions

XL: Conceptualization, data curation, formal analysis, investigation, methodology, visualization, writing: Original draft, writing: Review and editing. BL: Conceptualization, funding acquisition, project administration, resources, writing: Review and editing. XZ: Visualization, data curation, investigation. HQ: Resources, investigation. GL: Resources, investigation. CZ: Resources, investigation. All authors contributed to manuscript revision, read, and approved the submitted version.

Conflict of interest

Authors HQ and GL were employed by Fuli Lead Zinc Mine Co., Ltd. Author CZ was employed by Yunnan Tin Industry Group (Holding) Company Limted R & D Center.

The remaining authors declare that the research was conducted in the absence of any commercial or financial relationships that could be construed as a potential conflict of interest.

Publisher's note

References

Bao, Z., Li, Q., and Wang, C. Y. (2017). Metal source of giant Huize Zn-Pb deposit in SW China: New constraints from *in situ* Pb isotopic compositions of galena. *Ore Geol. Rev.* 91, 824–836. doi:10.1016/j.oregeorev.2017.08.019

Barker, S. L., Hickey, K. A., Cline, J. S., Dipple, G. M., Kilburn, M. R., Vaughan, J. R., et al. (2009). Uncloaking invisible gold: Use of nanoSIMS to evaluate gold, trace elements, and sulfur isotopes in pyrite from carlin-type gold deposits. *Econ. Geol.* 104, 897–904. doi:10.2113/gsecongeo.104.7.897

Canals, A., and Cardellach, E. (1997). Ore lead and sulphur isotope pattern from the low-temperature veins of the Catalonian Coastal Ranges (NE Spain). *Miner. Deposita* 32, 243–249. doi:10.1007/s001260050089

Chaussidon, M., Albarède, F., and Sheppard, S. M. F. (1989). Sulphur isotope variations in the mantle from ion microprobe analyses of micro-sulphide inclusions. *Earth Planet. Sci. Lett.* 92, 144–156. doi:10.1016/0012-821X(89)90042-3

Chen, F. (1979). The nature of mineral color. *Geol. Geochem.* 4, 10–16.

Claypool, G. E., Holser, W. T., Kaplan, I. R., Sakai, H., and Zak, I. (1980). The age curves of sulfur and oxygen isotopes in marine sulfate and their mutual interpretation. *Chem. Geol.* 28, 199–260. doi:10.1016/0009-2541(80)90047-9

Cook, N. J., Ciobanu, C. L., Pring, A., Skinner, W., Shimizu, M., Danyushevsky, L., et al. (2009). Trace and minor elements in sphalerite: A LA-ICPMS study. *Geochimica Cosmochimica Acta* 73, 4761–4791. doi:10.1016/j.gca.2009.05.045

Cui, Y., Zhou, J., Huang, Z., Luo, K., Nian, H., Lin, Y. E., et al. (2018). Geology, geochemistry and ore Genesis of the Fule Pb-Zn deposit, yunnan province, southwest China. *Acta Petrol. Sin.* 34, 194–206.

Deng, J., Wang, C., Bagas, L., Selvaraja, V., Jeon, H., Wu, B., et al. (2017). Insights into ore Genesis of the jinding Zn–Pb deposit, yunnan province, China: Evidence from Zn and *in-situ* S isotopes. *Ore Geol. Rev.* 90, 943–957. doi:10.1016/j.oregeorev.2016.10.036

Fleet, M. E., Chryssoulis, S. L., Stone, W. E., and Weisener, C. G. (1993). Partitioning of platinum-group elements and Au in the Fe–Ni–Cu–S system: Experiments on the fractional crystallization of sulfide melt. *Contributions Mineralogy Petrology* 115, 36–44. doi:10.1007/BF00712976

Fu, J., Hu, Z. C., Zhang, W., Yang, L., Liu, Y., Li, M., et al. (2016). *In situ*, sulfur isotopes (δ34S and δ33S) analyses in sulfides and elemental sulfur using high sensitivity cones combined with the addition of nitrogen by Laser Ablation MC-ICP-MS. *Anal. Chim. Acta* 911, 14–26. doi:10.1016/j.aca.2016.01.026

Hu, R., Fu, S., Huang, Y., Zhou, M., Fu, S., Zhao, C., et al. (2017). The giant South China Mesozoic low-temperature metallogenic domain: Reviews and a new geodynamic model. *J. Asian Earth Sci.* 137, 9–34. doi:10.1016/j.jseaes.2016.10.016

Hu, Y., Lin, Y. E., Chen, W. E. I., Huang, Z., and Wang, H. (2020). REE geochemistry of the hydrothermal calcites from the Huayuan orefield,in the Western Hunan,China. *Acta Mineral. Sin.* 40, 441–449.

Hu, Z. C., Zhang, W., Liu, Y. S., Gao, S., Li, M., Zong, K. Q., et al. (2015). Wave" signal-smoothing and mercury-removing device for laser ablation quadrupole and multiple collector ICPMS analysis: Application to lead isotope analysis. *Anal. Chem.* 87, 1152–1157. doi:10.1021/ac503749k

Huang, Z., Hu, R., Shu, W., Wen, H., Liu, S., and Fu, Y. (2011). A study on the large-scale low-temperature metallogenic domain in southwestern China—significance, history and new progress. Available at: http://ir.gyig.ac.cn/handle/352002/7069 (Accessed October 3, 2022).

Huang, Z. L., Chen, J., Han, R. S., Li, W. B., Liu, C. Q., Zhang, Z. L., et al. (2004). *Geochemistry and ore-formation of the huize giant lead-zinc deposit, yunnan province, China:discussion on the relationship between emeishan Flood basalts and lead-zinc mineralization*. Beijing, China: Geological Publishing House.

Jin, Z., Zhou, J., Zhilong, H., Luo, K., Jianguo, G., Song, P., et al. (2016). Ore Genesis of the Nayongzhi Pb-Zn deposit, Puding city, Guizhou province, China: Evidences from S and *in situ* Pb isotopes. *Acta Petrol. Sin.* 32, 3441–3455.

Jørgensen, B. B., Isaksen, M. F., and Jannasch, H. W. (1992). Bacterial sulfate reduction above 100 C in deep-sea hydrothermal vent sediments. *Science* 258, 1756–1757. doi:10.1126/science.258.5089.1756

Leach, D. L., Bradley, D., Lewchuk, M. T., Symons, D. T., de Marsily, G., and Brannon, J. (2001). Mississippi valley-type lead–zinc deposits through geological time: Implications from recent age-dating research. *Miner. Deposita* 36, 711–740. doi:10.1007/s001260100208

Leach, D. L., Taylor, R. D., Fey, D. L., Diehl, S. F., and Saltus, R. W. (2010). A deposit model for Mississippi Valley-type lead-zinc ores, *Chapter A mineral Depos. models Resour. Assess. USGS, Sci. Investigations Rep*.

Li, D., and Peng, M. (1990). Absorption spectrum and color nature of sphalerite. *Acta Mineral. Sin.* 10, 29–34.

Li, W., Huang, Z., and Yin, M. (2007). Dating of the giant huize Zn-Pb ore field of yunnan province, southwest China: Constraints from the Sm-Nd system in hydrothermal calcite. *Resour. Geol.* 57, 90–97. doi:10.1111/j.1751-3928.2006.00007.x

Li, Z. (2016). Geological geochemical characteristics and prospecting directions in the Fule lead-zinc deposit Yunnan Province.Master Degree Thesis, China University of Geosciences, Beijing, China.

Li, Z., Ye, L., Hu, Y., Wei, C., Huang, Z., Yang, Y., et al. (2020). Trace elements in sulfides from the Maozu Pb-Zn deposit, Yunnan Province, China: Implications for trace-element incorporation mechanisms and ore Genesis. *Am. Mineralogist* 105, 1734–1751. doi:10.2138/am-2020-6950

Liang, X., Li, B., Zhang, C., Qin, H., Li, G., and Zhang, X. (2022). Mineralogical and geochemical characteristics of carbonates and their geological significance to the Fuli Pb-Zn deposit, yunnan province. *Minerals* 12, 1317. doi:10.3390/min12101317

Liu, T. G., Lin, Y., Neng-pieng, S., and Jia-xi, Z. (2015). Cd content in sphalerite with different color. *Acta Mineral. Sin.* 35, 51–55.

Liu, Y. S., Hu, Z. C., Gao, S., Günther, D., Xu, J., Gao, C. G., et al. (2008). *In situ* analysis of major and trace elements of anhydrous minerals by LA-ICP-MS without applying an internal standard. *Chem. Geol.* 257, 34–43. doi:10.1016/j.chemgeo.2008.08.004

Ohmoto, H. G. M. B. (1997). Sulfur and carbon isotopes, *Geochem. Hydrothermal Ore Depos*. 8 517–611.

Ohmoto, H. (2018). "Stable isotope geochemistry of ore deposits," in *Stable isotopes in high temperature geological processes* (De Gruyter, Berlin, Germany), 491–560.

Ohmoto, H. (1972). Systematics of sulfur and carbon isotopes in hydrothermal ore deposits. *Econ. Geol.* 67, 551–578. doi:10.2113/gsecongeo.67.5.551

Ottaway, T., Wicks, F., Bryndzia, L., Kyser, T., and Spooner, E. (1994). Formation of the Muzo hydrothermal emerald deposit in Colombia. *Nature* 369, 552–554. doi:10.1038/369552a0

Ren, T., JiaXi, Z., Die, W., and GuangShu, Y. (2019). Trace elemental and S-Pb isotopic geochemistry of the Fule Pb-Zn deposit, NE Yunnan Province. *Acta Petrol. Sin.* 35, 3493–3505. doi:10.18654/1000-0569/2019.11.15

Seal, R. (2006). Sulfur isotope geochemistry of sulfide minerals. *Rev. Mineralogy Geochem.* 61, 633–677. doi:10.2138/rmg.2006.61.12

Si, R. (2005). Ore deposit geochemistryof the Fule dispersed element-polymetallic deposit. Yunnan province.*J. China univ. Geosciences*.doi:10.3390/min811051618: 351–352

Toulmin, P., Barton, P. B., and Wiggins, L. B. (1991). Commentary on the sphalerite geobarometer. *Am. Mineralogist* 76, 1038–1051.

Tu, G. Z., Gao, Z. M., and Hu, R. Z. (2003). *Dispersed element Geochemistry and metallogenic mechanism*,Beijing: Geological Publishing House Beijing, China 1–424.

Wei, C., Ye, L., Hu, Y., Danyushevskiy, L., Li, Z., and Huang, Z. (2019). Distribution and occurrence of Ge and related trace elements in sphalerite from the Lehong carbonate-hosted Zn-Pb deposit, northeastern Yunnan, China: Insights from SEM and LA-ICP-MS studies. *Ore Geol. Rev.* 115, 103175. doi:10.1016/j.oregeorev.2019.103175

Wei, C., Ye, L., Hu, Y., Huang, Z., Danyushevsky, L., and Wang, H. (2021). LA-ICP-MS analyses of trace elements in base metal sulfides from carbonate-hosted Zn-Pb deposits, South China: A case study of the maoping deposit. *Ore Geol. Rev.* 130, 103945. doi:10.1016/j.oregeorev.2020.103945

Xu, Y., Huang, Z., Zhu, D., and Luo, T. (2014). Origin of hydrothermal deposits related to the Emeishan magmatism. *Ore Geol. Rev.* 63, 1–8. doi:10.1016/j.oregeorev.2014.04.010

Yan, Z., Huang, Z., Xu, C., Chen, M., and Zhang, Z. (2007). Signatures of the source for the emeishan flood basalts in the ertan area: Pb isotope evidence. *Chin. J. Geochem.* 26, 207–213. doi:10.1007/s11631-007-0207-3

Yang, Q., Zhang, X., Ulrich, T., Zhang, J., and Wang, J. (2022). Trace element compositions of sulfides from Pb-Zn deposits in the Northeast Yunnan and northwest Guizhou Provinces, SW China: Insights from LA-ICP-MS analyses of sphalerite and pyrite. *Ore Geol. Rev.* 141, 104639. doi:10.1016/j.oregeorev.2021.104639

Ye, L., Li, Z. L., Hu, Y. S., Huang, Z. L., Zhou, J. X., Fan, H. F., et al. (2016). Trace elements in sulfide from the tianbaoshan Pb-Zn deposit, sichuan province, China: A LA-ICPMS study. *Acta Petrol. Sin.* 32, 3377–3393.

Ye, L., Cook, N. J., Ciobanu, C. L., Yuping, L., Qian, Z., Tiegeng, L., et al. (2011). Trace and minor elements in sphalerite from base metal deposits in SouthSouth China: A LA-ICPMS study. *Ore Geol. Rev.* 39, 188–217. doi:10.1016/j.oregeorev.2011.03.001

Zartman, R. E., and Doe, B. R. (1981). Plumbotectonics—the model. *Tectonophysics* 75, 135–162. doi:10.1016/0040-1951(81)90213-4

Yuan, B., Mao, J., Yan, X. H., Wu, Y., Zhang, F., and Zhao, L. L. (2014). Sources of metallogenic materials and metallogenic mechanism of Daliangzi Ore Field in Sichuan Province: Constraints from geochemistry of S, C, H, O, Sr isotope and trace element in sphalerite. *Acta Petrol. Sin.* 30, 209–220.

Zhang, C. (2008). The genetic model of Mississippi Valley-type deposits in the boundary area of Sichuan, Yunnan and Guizhou provinces. China.Doctor Dissertation, China University of Geosciences, Beijing, China.

Zhang, W., Hu, Z. C., Gunther, D., Liu, Y. S., Ling, W. L., Zong, K. Q., et al. (2016). Direct lead isotope analysis in Hg-rich sulfides by LA-MC-ICP-MS with a gas exchange device and matrix-matched calibration. *Anal. Chim. Acta* 948, 9–18. doi:10.1016/j.aca.2016.10.040

Zhang, W., Hu, Z. C., and Liu, Y. S. (2020). Iso-compass: New freeware software for isotopic data reduction of LA-MC-ICP-MS. *J. Anal. At. Spectrom.* 35, 1087–1096. doi:10.1039/D0JA00084A

Zhou, C., Yang, Z., Sun, H., Koua, K. A. D., and Lyu, C. (2022). LA-ICP-MS trace element analysis of sphalerite and pyrite from the Beishan Pb-Zn ore district, south China: Implications for ore Genesis. *Ore Geol. Rev.* 150, 105128. doi:10.1016/j.oregeorev.2022.105128

Zhou, J.-X., Huang, Z.-L., Zhou, M.-F., Zhu, X.-K., and Muchez, P. (2014). Zinc, sulfur and lead isotopic variations in carbonate-hosted Pb–Zn sulfide deposits, southwest China. *Ore Geol. Rev.* 58, 41–54. doi:10.1016/j.oregeorev.2013.10.009

Zhou, J.-X., Huang, Z., Zhu, D., Yan, Z., and Lv, Z. (2015). Geology, isotope geochemistry and geochronology of the Jinshachang carbonate-hosted Pb–Zn deposit, southwest China. *J. Asian Earth Sci.* 98, 272–284. doi:10.1016/j.jseaes.2014.11.024

Zhou, J.-X., Luo, K., Wang, X., Wilde, S., Wu, T., Huang, Z., et al. (2018a). Ore Genesis of the Fule Pb Zn deposit and its relationship with the emeishan large igneous province: Evidence from mineralogy, bulk C O S and *in situ* S Pb isotopes. *Gondwana Res.* 54, 161–179. doi:10.1016/j.gr.2017.11.004

Zhou, J.-X., Xiang, Z., Zhou, M., Feng, Y., Luo, K., Huang, Z., et al. (2018b). The giant Upper Yangtze Pb–Zn province in SW China: Reviews, new advances and a new genetic model. *J. Asian Earth Sci.* 154, 280–315. doi:10.1016/j.jseaes.2017.12.032

Zhou, J., Huang, Z., and Yan, Z. (2013a). The origin of the Maozu carbonate-hosted Pb–Zn deposit, southwest China: Constrained by C–O–S–Pb isotopic compositions and Sm–Nd isotopic age. *J. Asian Earth Sci.* 73, 39–47. doi:10.1016/j.jseaes.2013.04.031

Zhou, J., Huang, Z., Zhou, G., Li, X., Ding, W., and Bao, G. (2010). Sulfur isotopic composition of the Tianqiao Pb-Zn ore deposit, Northwest Guizhou Province, China: Implications for the source of sulfur in the ore-forming fluids. *Chin. J. Geochem.* 29, 301–306. doi:10.1007/s11631-010-0460-8

Zhou, J., Huang, Z., Zhou, M., Li, X., and Jin, Z. (2013b). Constraints of C–O–S–Pb isotope compositions and Rb–Sr isotopic age on the origin of the Tianqiao carbonate-hosted Pb–Zn deposit, SW China. *Ore Geol. Rev.* 53, 77–92. doi:10.1016/j.oregeorev.2013.01.001

Zhou, J. X., Huang, Z. L., Jg, G., and Yan, Z. F. (2013c). Geological and C-O-S-Pb-Sr isotopic constraints on the origin of the Qingshan carbonate-hosted Pb-Zn deposit, Southwest China. *Int. Geol. Rev.* 55, 904–916. doi:10.1080/00206814.2013.767496

Zhou, J. X., Zl, H., and Bao, G. P. (2013d). Geological and sulfur-lead-strontium isotopic studies of the Shaojiwan Pb-Zn deposit, SouthwestChina: Implications for the origin of hydrothermal fluids. J. Geochem. *Explor.* 128, 51–61. doi:10.1016/j.gexplo.2013.01.007

Zong, K. Q., Klemd, R., Yuan, Y., He, Z. Y., Guo, J. L., Shi, X. L., et al. (2017). The assembly of Rodinia: The correlation of early Neoproterozoic (ca. 900 Ma) high-grade metamorphism and continental arc formation in the southern Beishan Orogen, southern Central Asian Orogenic Belt (CAOB. *Precambrian Res.* 290, 32–48. doi:10.1016/j.precamres.2016.12.010